Proceedings of the Project Review, Geo-Mathematical Imaging Group (Purdue University, West Lafayette IN), Vol. 1 (2012) pp. 189-208.

SHAPE OPTIMIZATION IN FULL WAVEFORM INVERSION WITH SPARSE BLOCKY MODEL REPRESENTATIONS

ZHAOHUI GUO* AND MAARTEN V. DE HOOP†

Abstract. We present a variational framework for shape optimization and shape reconstruction problems in seismic domains based full waveform inversion. We discuss general shape functionals in this framework, along with applications to shape optimization using the Helmholtz equation and image domain segmentation. We study the shape derivative in each case to express the variation of energy with respect to the geometric boundary deformations. Moreover, we present some numerical experiments of the problem of salt body recovery for seismic full waveform inversion in the frequency domain. The level set method is implemented to track the dynamic evolution of shape changes, with the descent direction derived from the shape derivative.

Key words. Inverse problem, shape optimization, variational methods, gradient flow, TV regularization, level set method.

1. Introduction. We consider an inverse boundary value problem for the Helmholtz equation from an optimization point of view. In particular, we study full waveform inversion in reflection seismology [32, 33, 40, 43, 45] with the goal to reconstruct wavespeed variations in the subsurface of the earth. Such an inversion is typically based on an iteration, like the Landweber iteration [20], the convergence of which has been analyzed recently [14, 16, 17, 37]. In this analysis, the Dirichlet-to-Neumann map [44] is viewed as the data, but here we formulate the inverse problem essentially in terms of a single-layer potential operator. To facilitate the convergence of the iteration, we introduce a hybrid parametrization of the models approximating the variations in wavespeed in the subsurface consistent with the conditions of convergence of the mentioned Landweber iteration. Essentially, we subdivide the models into domains, each of which has a distinct character expressed in terms of local wavespeed fluctuations and structure. We anticipate the domains to be an imprint of the local geology of the subsurface, and use an adaptive basis to represent the local wavespeed variations. (This strategy can be generalized to the use of adaptive frames in general and aggregated wavelet frames in particular [9, 8].) As a key example, we mention salt bodies, with rather homogeneous, high wavespeeds and sharp boundaries versus surrounding sedimentary layers exhibiting a structure containing closely spaced interfaces. In the iteration we propose, we alternate between an optimization for the wavespeed functions, an edge-based segmentation yielding a (further) subdivision into domains, and an optimization for the shapes of the domains, see Figure 1. Moreover we incorporate a total variation (TV) regularization motivated by the desire to approximate the wavespeed by piecewise constant functions.

Full waveform inversion in the presence of salt bodies has been a major challenge in exploration seismology. Reasons for this include the complication in obtaining an initial model which guarantees convergence of the iteration, and the sensitivity to smoothing the sharp salt boundaries. We mitigate these issues by incorporating the salt boundaries, keeping them sharp, explicitly as part of the inverse problem on the one hand, and implicitly promoting sparse model representations on the other hand. A related approach can be found in Shin [39].

We make use of a segmentation technique well established in [21]. We adapt the shape optimization developed in obstacle scattering from the work of [36] to our inverse problem for the Helmholtz equation. We derive the derivatives of the relevant functionals using Lagrange multipliers. We formulate these optimizations in terms of level set functions [28, 27] and arrive at an integrated framework for carrying out the iterations.

Our approach is the following; see Figure 1 for a diagram. We first consider the problem of determining the wavespeed, q, in a bounded domain in the context of a multi-frequency boundary value inverse problem for the Helmholtz equation. The wavespeed has conormal singularities. The domain is assumed to be naturally segmented into subregions Ω_j; in each subregion, the character

*Department of Mathematics, Purdue University, West Lafayette IN 47907, USA (zhaohuig@gmail.com)
†Department of Mathematics, Purdue University, West Lafayette IN 47907, USA (mdehoop@purdue.edu)

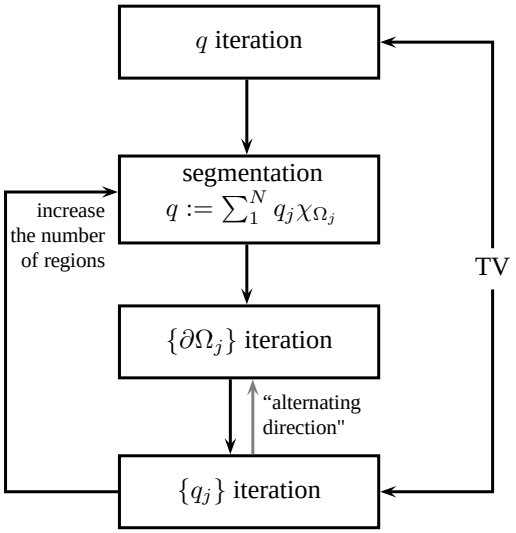

FIG. 1. *Our scheme for full waveform inversion based on adaptive decomposition into subdomains.*

of wavespeed variations is distinct and we write $q := \sum_1^N q_j \chi_{\Omega_j}$. Thus we cast the inverse problem into a joint inverse problem for the number and shapes of the domains (the boundaries of which correspond with conormal singularities) and for the wavespeed variations within these domains using methods of constrained and shape optimization. This point of view is intimately connected to the strategy of imposing sparsity of the representations of the wavespeed models, where the "basis" for the representations is adapted or guided in the iteration process using level sets and TV regularization. We develop a basic gradient-based "alternating direction" type approach to update the $\{\partial\Omega_j\}$ and $\{q_j\}$.

Methods based on the Fréchet derivative of an operator L which maps a set of admissible boundaries onto the far field scattering data were developed by [15, 18, 31]. The optimization strategy in [18, 19, 30] is based on a gradient type of method which needs the derivative of the operator L with respect to the admissible domains. These methods all assume the domain to be star shaped. Therefore, the obstacle representation is limited. Physical optics based shape reconstruction of voids was introduced by [22]. Santosa [36] proposed an approach for general classes of inverse problems involving the reconstruction of obstacle shapes using the level set method. The algorithm in his approach solves the minimization of a least-square functional to obtain a boundary evolution. Further applications and extensions of this shape optimization method can be found in [10, 23, 34]. Burger [5] further developed a functional-analytic framework for the construction of level set methods for shape optimization and reconstruction. In our shape optimization, we use a velocity method derived from the variational models, where the velocity is defined as the gradient flow for a corresponding energy functional.

The outline of the paper is as follows. In Section 2 we present the image based and data based shape functionals and the associated shape derivatives. We give general representations and describe the discretization scheme used to calculate the descent direction. In Section 3 we express the derivative of the shape functional in terms of solutions of the Helmholtz equation using the adjoint state method. We review the edge-based segmentation shape functional and its derivative in Section 4. In Section 5 we summarize our algorithm and carry out numerical experiments. We end the paper with some conclusions.

2. Shape optimization. We begin with considering general shape functionals, image-based $\mathcal{J}(\Omega)$, and data-based $\mathcal{J}(\Omega, u(\Omega))$, which depend on a connected domain $\Omega \subset \Theta$, where Θ is a

bounded domain in $\mathbb{R}^n$; in our applications, $n = 2$ or 3. The boundary of Ω, $\Gamma = \partial\Omega$, is assumed to be of class $C^{1,1}$. We denote the outward normal to Γ by ν and the curvature of Γ is κ. Furthermore, $u(\Omega)$ is a solution of the Helmholtz equation in a configuration containing Ω.

2.1. Shape deformation. To describe the evolution of the shape of Ω, we consider a general transformation, $t \mapsto T_t$, in $C^1([0,\varepsilon))$ for some $\varepsilon > 0$, such that $x_t = T_t(x)$. In general, the velocity field at the point x_t is defined in Eulerian coordinates: $V(x,t) \in C([0,\varepsilon); C^k(\bar{\Theta}; \mathbb{R}^n))$ for some k, has the form

$$V(x,t) = \left(\frac{\mathrm{d}T_t}{\mathrm{d}t}\right) \circ T_t^{-1}(x).$$

Let x_t denote the solution of the following ordinary differential equation

$$\frac{\mathrm{d}x_t}{\mathrm{d}t} = V. \tag{2.1}$$

The shape deformation can be linearly expressed as

$$x_t = x + tV, \tag{2.2}$$

for a given vector field V.

Assuming that $V = 0$ outside a small neighborhood of Γ, we define the perturbed sets

$$\Gamma_t = T_t(\Gamma) = \{T_t(x) \mid x \in \Gamma\}, \quad \Omega_t = T_t(\Omega) = \{T_t(x) \mid x \in \Omega\}. \tag{2.3}$$

2.2. Shape functional and shape derivative. We consider two general forms for the energy functionals: the first form is given by

$$\mathcal{J}(\Omega) = \int_\Omega \Phi(x)\mathrm{d}x + \int_\Gamma \Psi(x)\mathrm{d}\sigma. \tag{2.4}$$

The second form is obtained, essentially, by replacing $\Phi(x)$ by $\Phi(x, u(\Omega))$ and $\Psi(x)$ by $\Psi(x, u(\Gamma))$, where $u(\Omega)$ or $u(\Gamma)$ solves a problem like (3.1). However, in our application, we consider the specific form,

$$\mathcal{J}(\Omega) = \mathcal{J}(\Omega, u(\Omega)) = \int_\Sigma \varphi(u(\Omega) - d)\mathrm{d}\sigma, \tag{2.5}$$

where Σ encloses Ω, and φ is a non-negative function inducing a norm; $u(\Omega)$ is a solution of the Helmholtz equation in a configuration containing a subdomain Ω as before. These functionals can be supplemented with regularization. A basic regularization strategy adds a term $\gamma H^{n-1}(\Gamma)$ to the right-hand sides above, where $\gamma > 0$ is a parameter and $H^{n-1}(\Gamma)$ is the $(n-1)$-dimensional Hausdorff measure [12, 25].

The shape derivatives of functionals $\mathcal{J}(\Omega)$ are given by

$$D\mathcal{J}(\Omega)\, V = \lim_{t\to 0} \frac{\mathcal{J}(\Omega_t) - \mathcal{J}(\Omega)}{t}. \tag{2.6}$$

In general, we can represent these as

$$D\mathcal{J}(\Omega)\, V = (\rho, v)_{L^2(\Gamma)}, \tag{2.7}$$

for some $\rho \in L^2(\Gamma)$, with $v = V \cdot \nu$ in Γ. The shape derivative is insensitive to the tangential component of the boundary velocity, because the shape does not change in the tangential component of transformation. Typically, if $\mathcal{J}$ is given by a volume integral one obtains a boundary integral; the curvature of Γ, κ say, plays a role when the energy functional involves a boundary integral, through regularization, as in [41].

After the shape derivative is obtained, the gradient flow can be chosen to optimize the energy functional. We let $\mathcal{V}$ be a subspace of $L^2(\Gamma)$ equipped with an inner product $\langle .,. \rangle$, and $\tilde{v}$ be the solution to

$$\langle \tilde{v}, v \rangle = -(\rho, v)_{L^2(\Gamma)} =: -D\mathcal{J}(\Omega)\, V \quad \text{for all } v \in \mathcal{V}. \tag{2.8}$$

For more general spaces, $\langle .,. \rangle$ is a bilinear form (continuous and coercive) defining a duality pairing $(\mathcal{V}', \mathcal{V})$. $D\mathcal{J}(\Omega)$ signifies the gradient in the norm on $\mathcal{V}$, while $D\mathcal{J}(\Omega)\,\tilde{V} = -\langle \tilde{v}, \tilde{v} \rangle$ with $\tilde{V} = \tilde{v}\nu$, and $\tilde{v}$ is the *gradient descent* direction. The most basic example is $\mathcal{V} = L^2(\Gamma)$, which gives a natural choice of $\tilde{v} = -\rho$ in Γ, but we will also consider $\mathcal{V} = H^1(\Gamma)$. If $\mathcal{B}$ is an elliptic differential operator such that $(\mathcal{B}v, \tilde{v})_{L^2(\Gamma)} = \langle v, \tilde{v} \rangle$, then the gradient flow is called the $\mathcal{B}$-gradient flow. We obtain a partial differential equation on Γ for $\tilde{v}$: $\mathcal{B}\tilde{v} = -\rho$.

Since the shape derivatives of the energy functionals in (2.4) and (2.5) can be written in the form of (2.7), one can choose to use the normal velocity field $\tilde{V} = \tilde{v}\,\nu$ on Γ with an continuous extension to the entire domain.

2.3. Level set methods. We introduce the level set approach to represent domains and their boundaries with a numerical implementation of optimization in mind. The method was first introduced by Osher and Sethian in [28]. The main idea is to formulate a boundary as the zero level set of a higher dimensional level set function. Thus the motion of a boundary can be formulated as the evolution of a level set function, $\phi(x,t)$ say, which is a Lipschitz continuous function, according to

$$\Gamma_t = \{x \mid \phi(x,t) = 0\}, \quad \Omega_t = \{x \mid \phi(x,t) < 0\}. \tag{2.9}$$

We denote the outward normal to Ω_t by ν_t. We identify the initial domain Ω_0 with Ω and boundary Γ_0 with Γ. We note that

$$\nu_t(x) = \frac{\nabla\phi(x,t)}{|\nabla\phi(x,t)|}, \quad x \in \Gamma_t.$$

The evolution of Γ_t is prescribed through a normal velocity $v(x,t)$,

$$\frac{\partial\phi}{\partial t} = -v(x,t)\,|\nabla\phi|. \tag{2.10}$$

That is, if $\phi(x_t,t) = 0$, then

$$v(x_t,t) = \frac{\nabla\phi(x_t,t)}{|\nabla\phi(x_t,t)|} \cdot \frac{\mathrm{d}x_t}{\mathrm{d}t}; \quad \frac{\mathrm{d}x_t}{\mathrm{d}t} = V(x_t,t) \tag{2.11}$$

supplemented with the initial condition $x_0 = x$. With level sets, we can track the dynamic evolution of boundaries and the deformation of shapes, even with topological changes, such as splitting and merging. Thus we can allow the domain Ω_t to break up into subdomains and Ω_t need not to be connected.

Standard level set methods can develop irregularities, e.g. very sharp or flat boundaries during the evolution, which makes further computation highly inaccurate and unstable. To avoid these problems, a numerical scheme known as re-initialization was proposed in [27, 38, 42]. In this scheme, one initializes the function ϕ by a signed distance function,

$$\frac{\partial\psi}{\partial t} = \mathrm{sign}(\phi)\,(1 - |\nabla\psi|). \tag{2.12}$$

The re-initialized level set function $\psi(x,t)$ has the same zero level set Γ_t as $\phi(x,t)$ and satisfies $|\nabla\psi| = 1$. In practice, re-initialization has to be performed many times to maintain the stable evolution and accurate solution.

Moreover, velocity must be constructed not only on the moving interface Γ_t, but in the entire domain. The methods of velocity extension include simple extrapolation [24], or solving an advection equation combined with the re-initialization procedure [7, 29]. v can also be obtained through the fast matching method as in [2]. On the other hand, the narrowband method [1] is used in the numerical implementation. The main idea is to only update the grid points lying within a given distance to the zero level sets and neglect all other sample points, which highly reduces the computational cost.

Li [21] proposed a new technique of level set evolution called distance regularized level set evolution (DRLSE). Following his work, we add a penalty term

$$\mathcal{R}_p(\phi) = \int_\Theta p(|\nabla\phi|)\,\mathrm{d}x, \tag{2.13}$$

to the energy functional to maintain the signed distance property. Here, the potential function $p(s)$ must be chosen to have a minimum at $s = 1$, to keep the property $|\nabla\phi| = 1$. We note that neither re-initialization nor velocity extension procedures are needed in the DRLSE implementation due to the intrinsic distance regularization effect in the level set evolution.

2.4. Time discretization. Here, we consider the discretization in t. We denote the time step by τ_n. The forward Euler scheme for the gradient flow is then given by (cf. (2.1), (2.8))

$$x_{n+1} = x_n + \tau_n V_n;$$

in the level set formulation, we obtain (cf. (2.10))

$$\phi^{n+1} = \phi^n - \tau_n v_n |\nabla\phi^n|.$$

In view of regularization terms, we may encounter the mean curvature κ generated by boundary terms in the shape derivative of $\mathcal{J}(\Omega)$. For stability, based on second order spatial derivatives, the Courant-Friedrichs-Lewy condition roughly requires the time discretization step to be proportional to the square of the minimum space discretization parameter. In this case, one resorts to implicit schemes, such as the implicit Euler approximation,

$$x_{n+1} = x_n + \tau_n V_{n+1}.$$

Motivated by the implicit Euler method for the heat equation, one considers the following variational problem [3, 5]:

$$\Omega_{n+1} = \arg\min_\Omega \left[\mathcal{J}(\Omega) + \frac{1}{2\tau_n} d^2(\Omega, \Omega_n)\right], \tag{2.14}$$

where the second term measures the difference between Ω and Ω_n, which can be expressed in terms of τ_n and V_{n+1}. In addition, this idea corresponds to the generalized iterated Tikhonov regularization.

Suppose Ω_{n+1} deformed by $V_{n+1} = v_{n+1}\nu_{n+1}$ is the solution of the minimization problem, with

$$d^2(\Omega_{n+1}, \Omega_n) = \langle \tau_n v_{n+1}, \tau_n v_{n+1}\rangle.$$

Then

$$\Omega_{n+1} = \arg\min_\Omega \left[\mathcal{J}(\Omega) + \frac{\tau_n}{2}\langle v_{n+1}, v_{n+1}\rangle\right] \tag{2.15}$$

and the first order optimality conditions give

$$(\rho_{n+1}, \tilde{v})_{L^2(\Gamma_{n+1})} + \langle v_{n+1}, \tilde{v}\rangle = 0 \quad \text{for all } \tilde{v} \in \mathcal{V}_{n+1}.$$

This coincides with the regularized gradient flow (2.8), up to an implicit time discretization.

Both in $L^2(\Gamma)$ and $H^1(\Gamma)$, v_{n+1} is computed via a partial differential equation: $\mathcal{B}v_{n+1} = -\rho_{n+1}$, in which ρ_{n+1} is unknown. One method to overcome this problem, as proposed by [11], is to linearize and replace the unknown Ω_{n+1} and Γ_{n+1} by the known Ω_n and Γ_n. Then

$$\langle v_{n+1}, \tilde{v}\rangle = -(\rho_n, \tilde{v})_{L^2(\Gamma_n)} \quad \text{for all } \tilde{v} \in \mathcal{V}.$$

However, if one chooses

$$V_{n+1} = v_{n+1}\nu_n = -\rho_n\nu_n,$$

then we recover the explicit scheme, which has the shortcoming of requiring a small time step.

An alternative approach is based on applying an implicit-explicit scheme. This approach works by applying different schemes to different terms in the discretization. We split ρ into two parts, $\rho = \rho^E + \rho^I$. For those terms in ρ^E which require larger time steps, we apply the standard explicit discretization scheme, while for those terms in ρ^I with strict time step size restrictions, we use an implicit scheme. This provides a stable scheme involving an overall time step proportional to the space step size. For example, as mentioned before, by adding a regularization term $\gamma\int_\Gamma \mathrm{d}\sigma$, the shape derivative acquires a curvature term, $\rho^I = \gamma\kappa$, and can be represented as

$$D\mathcal{J}(\Omega)\,V = (\rho^E + \gamma\kappa, v)_{L^2(\Gamma)}. \tag{2.16}$$

Following the mentioned strategy, we obtain

$$\mathcal{B}v_{n+1} + \gamma\kappa_{n+1} = -\rho_n^E,$$

which involves solving a system of linear equations at every time step.

The time step size can be adaptively chosen using a backtracking line search, finding the locally optimal τ_n for every iteration. In practice, it can be time consuming to perform the line search. Thus one can use a fixed step size at the cost of slow convergence.

3. The shape derivative of the data-based functional. In this section, we study the shape derivative of a shape functional based on the solution of a Helmholtz equation. We obtain an explicit expression for the shape derivative which can be numerically implemented.

We consider time-harmonic waves, described by the solution u of a Helmholtz equation on $\mathbb{R}^n$, for $n \geq 2$. We write

$$q(x) = \omega^2 c^{-2}(x),$$

$\omega \in \mathbb{R}$. We introduce a bounded open domain Θ with boundary in $C^{(1,1)}$ and assume that $\Theta' = \mathbb{R}^n\backslash\overline{\Theta}$ is connected. The wavefield u takes u^+ and u^- as the limit from the exterior and interior of Γ. Moreover, we introduce a domain $\Omega \subset \Theta$ with boundary Γ, and consider the partitioned boundary value problem as in [6]

$$\left\{\begin{array}{rcll} (-\Delta - \quad q_0)u &=& 0, \quad x \in \Theta' & , \\ (-\Delta - q_2(x))u &=& f, \quad x \in \Theta\backslash\overline{\Omega} & , \\ (-\Delta - q_1(x))u &=& 0, \quad x \in \Omega & , \\ u^- - u^+ &=& 0, \quad x \in \Gamma & , \\ \dfrac{\partial u^-}{\partial\nu} - \dfrac{\partial u^+}{\partial\nu} &=& 0, \quad x \in \Gamma & , \\ \lim\limits_{r\to\infty}\left(r\dfrac{\partial u}{\partial r} - \mathrm{i}\sqrt{q_0}u\right) &=& 0 & . \end{array}\right. \tag{3.1}$$

Here,

$$L^\infty(\Theta) \ni \left\{\begin{array}{ll} q_1(x) & \text{if } x \in \Omega \\ q_2(x) & \text{if } x \in \Theta\backslash\overline{\Omega} \end{array}\right.$$

while $q_0 = \omega^2 c_0^{-2}$, where c_0 is constant. Furthermore, $f \in H^{-1}(\Theta)$ represents a volume source.

We replace (3.1) by the equivalent problem on Θ,

$$\left\{\begin{array}{rcll} (-\Delta - q_2(x))u &=& f, \quad x \in \Theta\backslash\overline{\Omega} & , \\ (-\Delta - q_1(x))u &=& 0, \quad x \in \Omega & , \\ u^- - u^+ &=& 0, \quad x \in \Gamma & , \\ \dfrac{\partial u^-}{\partial \nu} - \dfrac{\partial u^+}{\partial \nu} &=& 0, \quad x \in \Gamma & , \\ \dfrac{\partial u}{\partial \nu} &=& -\Lambda_e u, \quad x \in \partial\Theta & , \end{array}\right. \tag{3.2}$$

where Λ_e is the exterior Dirichlet-to-Neumann map [44] for the Helmholtz equation on Θ'. We introduce an open bounded domain D, with $\Omega \subset D \subset \Theta$ and a boundary in $C^{(1,1)}$, and $D' = \mathbb{R}^3\backslash\overline{D}$ being connected. Let Σ be a open portion of ∂D, and suppose $\mathrm{supp}(f) \subseteq \Theta\backslash\overline{D}$.

The solution u of (3.2), in $H^1(\Theta)$, also solves the variational equation

$$b(\Omega; u, v) = s(v) \quad \text{for all } v \in H^1(\Theta), \tag{3.3}$$

where

$$b(\Omega; u, v) = \int_{\Theta\backslash\overline{\Omega}} (\nabla u \cdot \nabla \bar{v} - q_2\, u\bar{v})\, \mathrm{d}x + \int_{\Omega} (\nabla u \cdot \nabla \bar{v} - q_1\, u\bar{v})\, \mathrm{d}x \tag{3.4}$$

and

$$s(v) = \int_{\Theta\backslash\overline{D}} f\, \bar{v}\, \mathrm{d}x - \int_{\partial\Theta} (\Lambda_e u)\, \bar{v}\, \mathrm{d}\sigma. \tag{3.5}$$

We introduce the shape deformation, $\Omega_t = T_t(\Omega)$, where $T_t(x) = x + tV(x)$, and the vector field $V = 0$ outside a small neighborhood of $\Gamma = \partial\Omega$. We write the variational equation in the case Ω is replaced by Ω_t in terms of coordinates x_t,

$$b(\Omega_t; u_t, v) = s(v) \quad \text{for all } v \in H^1(\Theta), \tag{3.6}$$

where

$$b(\Omega_t; u_t, v) = \int_{\Theta\backslash\overline{\Omega_t}} (\nabla_x u_t \cdot \nabla_x \bar{v} - q_2\, u_t \bar{v})\, \mathrm{d}x_t + \int_{\Omega_t} (\nabla_x u_t \cdot \nabla_x \bar{v} - q_1\, u_t \bar{v})\, \mathrm{d}x_t, \tag{3.7}$$

using variables of integration x_t. We write explicitly the solution operator $u_t = \mathcal{S}(\Omega_t; q_1, q_2)f$ and introduce the shape functional

$$\mathcal{J}(\Omega_t, q_1, q_2) = \frac{1}{2}\|\mathcal{P}(\mathcal{S}(\Omega_t; q_1, q_2)f - d_f)\|^2_{L^2(\Sigma)}. \tag{3.8}$$

Here, d_f represents the data, $\mathcal{P}$ is an elliptic operator such that $\|\mathcal{P}\, d\|_{L^2(\Sigma)} = \|d\|_{H^{3/2}(\Sigma)}$. Taking the derivative with respect to t yields

$$\frac{\mathrm{d}}{\mathrm{d}t}\mathcal{J}(\Omega_t, q_1, q_2)\,\Big|_{t=0} = \mathrm{Re}\int_{\Sigma} [\mathcal{P}^*\mathcal{P}(\mathcal{S}(\Omega_t; q_1, q_2)f - d_f)]\; \frac{\mathrm{d}}{\mathrm{d}t}\mathcal{S}(\Omega_t; q_1, q_2)f\,\Big|_{t=0}\, \mathrm{d}\sigma. \tag{3.9}$$

To avoid the explicit evaluation of $\frac{\mathrm{d}}{\mathrm{d}t}\mathcal{S}(\Omega_t; q_1, q_2)f$, we introduce a Lagrange multiplier w and a family of functionals

$$\begin{aligned} \mathcal{L}(\Omega_t; v, w) &= \mathcal{J}(\Omega_t, q_1, q_2) + \mathrm{Re}\,(b(\Omega_t; v, w) - s(w)), \\ &= \frac{1}{2}\|\mathcal{P}(v - d_f)\|^2_{L^2(\Sigma)} + \mathrm{Re}\,(b(\Omega_t; v, w) - s(w)). \end{aligned} \tag{3.10}$$

If $v = u_t$ is the solution of the direct problem (3.6),

$$\mathcal{L}(\Omega_t; u_t, w) = \mathcal{J}(\Omega_t, q_1, q_2) \quad \text{for all } w \in H^1(\Theta)$$

and the shape derivative of $\mathcal{J}$ in the direction V is given by

$$D\mathcal{J}(\Omega, q_1, q_2)\, V = \frac{\mathrm{d}}{\mathrm{d}t}\mathcal{L}(\Omega_t, u_t, w)\,\Big|_{t=0} \quad \text{for any } w \in H^1(\Theta), \tag{3.11}$$

where

$$\begin{aligned}\frac{\mathrm{d}}{\mathrm{d}t}\mathcal{L}(\Omega_t, u_t, w)\,\Big|_{t=0} = \mathrm{Re}\,\Big\{ \Big[\int_\Sigma [\mathcal{P}^*\mathcal{P}(\mathcal{S}(\Omega_t; q_1, q_2)f - d_f)]\ \frac{\mathrm{d}}{\mathrm{d}t}\mathcal{S}(\Omega_t; q_1, q_2)f\,\Big|_{t=0}\,\mathrm{d}\sigma \\ + b\left(\Omega; \frac{\mathrm{d}}{\mathrm{d}t}\mathcal{S}(\Omega_t; q_1, q_2)f\,\Big|_{t=0}, w\right)\Big] + \frac{\mathrm{d}}{\mathrm{d}t}b(\Omega_t; u, w)\,\Big|_{t=0}\Big\}.\end{aligned}$$

If w solves

$$b(\Omega; v, w) = -\int_\Sigma [\mathcal{P}^*\mathcal{P}(\mathcal{S}(\Omega_t; q_1, q_2)f - d_f)]\ v\,\mathrm{d}\sigma \quad \text{for all } v \in H^1(\Theta), \tag{3.12}$$

then

$$\frac{\mathrm{d}}{\mathrm{d}t}\mathcal{L}(\Omega_t, u_t, w)\,\Big|_{t=0} = \mathrm{Re}\,\Big\{ \frac{\mathrm{d}}{\mathrm{d}t}b(\Omega_t; u, w)\,\Big|_{t=0}\Big\}. \tag{3.13}$$

We can write (3.12) in the form of the direct problem:

$$b(\Omega; \bar{w}, v) = -\int_\Sigma [\mathcal{P}^*\mathcal{P}(\mathcal{S}(\Omega_t; q_1, q_2)f - d_f)]\ \bar{v}\,\mathrm{d}\sigma \quad \text{for all } v \in H^1(\Theta); \tag{3.14}$$

here, $\bar{w} \in H^1(\Theta)$ is the so-called adjoint state, and is the solution to

$$\left\{\begin{array}{rcll} (-\Delta - \quad q_0)\bar{w} &=& 0, \quad x \in \Theta' & , \\ (-\Delta - q_2(x))\bar{w} &=& [\mathcal{P}^*\mathcal{P}(\mathcal{S}(\Omega_t; q_1, q_2)f - d_f)]\ \delta_\Sigma, \quad x \in \Theta\backslash\overline{\Omega} & , \\ (-\Delta - q_1(x))\bar{w} &=& 0, \quad x \in \Omega & , \\ \bar{w}^- - \bar{w}^+ &=& 0, \quad x \in \Gamma & , \\ \dfrac{\partial \bar{w}^-}{\partial \nu} - \dfrac{\partial \bar{w}^+}{\partial \nu} &=& 0, \quad x \in \Gamma & , \\ \lim\limits_{r\to\infty}\left(r\dfrac{\partial \bar{w}}{\partial r} - \mathrm{i}\sqrt{q_0}\bar{w}\right) &=& 0 & . \end{array}\right. \tag{3.15}$$

Again, we have the equivalent problem

$$\left\{\begin{array}{rcll} (-\Delta - q_2(x))\bar{w} &=& [\mathcal{P}^*\mathcal{P}(\mathcal{S}(\Omega_t; q_1, q_2)f - d_f)]\ \delta_\Sigma, \quad x \in \Theta\backslash\overline{\Omega} & , \\ (-\Delta - q_1(x))\bar{w} &=& 0, \quad x \in \Omega & , \\ \bar{w}^- - \bar{w}^+ &=& 0, \quad x \in \Gamma & , \\ \dfrac{\partial \bar{w}^-}{\partial \nu} - \dfrac{\partial \bar{w}^+}{\partial \nu} &=& 0, \quad x \in \Gamma & , \\ \dfrac{\partial \bar{w}}{\partial \nu} &=& -\Lambda_e\bar{w}, \quad x \in \partial\Theta & . \end{array}\right. \tag{3.16}$$

We have made use of the fact that $\Lambda_e^*(\bar{w}) = \overline{\Lambda_e w}$, and w^+, w^- are defined in the same way as u^+, u^-.

We now evaluate $\frac{\mathrm{d}}{\mathrm{d}t} b(\Omega_t; u, w)|_{t=0}$. We consider the change of variables of integration, $x_t \to x$, following the deformation of the domain: We introduce

$$F_t = \nabla T_t = I + t\,\nabla V,$$

so that

$$T_t^*(\nabla_{x_t} u_t) = F_t^{-T} \nabla (T_t^* u_t), \quad \mathrm{d}x_t = \det F_t \,\mathrm{d}x,$$

while

$$\frac{\mathrm{d}}{\mathrm{d}t} F_t \,\Big|_{t=0} = \nabla V, \quad \frac{\mathrm{d}}{\mathrm{d}t} \nabla_{x_t} u_t \,\Big|_{t=0} = -(\nabla V)^T \nabla u_t(T_t(.)), \quad \frac{\mathrm{d}}{\mathrm{d}t} \mathrm{d}x_t \,\Big|_{t=0} = \nabla \cdot V \,\mathrm{d}x.$$

(We also have $\nu_t \mathrm{d}\sigma_t = \det F_t \; \nu \,\mathrm{d}\sigma \cdot F_t^{-1}$.) Then

$$\begin{aligned} (3.17) \qquad & \frac{\mathrm{d}}{\mathrm{d}t} b(\Omega_t; u, w) \,\Big|_{t=0} \\ & = \int_{\Theta \setminus \overline{\Omega}} (\nabla u \cdot \nabla \bar{w} - q_2\, u \bar{w})\, \nabla \cdot V \,\mathrm{d}x - \int_{\Theta \setminus \overline{\Omega}} ((\nabla V + (\nabla V)^T) \nabla u) \cdot \nabla \bar{w} \,\mathrm{d}x + \\ & \quad + \int_{\Omega} (\nabla u \cdot \nabla \bar{w} - q_1\, u \bar{w})\, \nabla \cdot V \,\mathrm{d}x - \int_{\Omega} ((\nabla V + (\nabla V)^T) \nabla u) \cdot \nabla \bar{w} \,\mathrm{d}x. \end{aligned}$$

We consider the integrals over Ω. We have

$$\begin{aligned} \int_{\Omega} (\nabla u \cdot \nabla \bar{w} - q_1\, u \bar{w})\, \nabla \cdot V \,\mathrm{d}x = & - \int_{\Omega} \nabla (\nabla u \cdot \nabla \bar{w} - q_1\, u \bar{w}) \cdot V \,\mathrm{d}x \\ & - \int_{\Gamma} \nabla u^- \cdot \nabla \bar{w}^- \, \nu \cdot V \,\mathrm{d}\sigma + \int_{\Gamma} q_1\, u^- \bar{w}^- \, \nu \cdot V \,\mathrm{d}\sigma \end{aligned}$$

and

$$\begin{aligned} - \int_{\Omega} ((\nabla V + (\nabla V)^T) \nabla u) \cdot \nabla \bar{w} \,\mathrm{d}x = & \int_{\Omega} [(\nabla \cdot \nabla u)\, V \cdot \nabla \bar{w} + (V \cdot \nabla u)\, \nabla \cdot \nabla \bar{w}] \,\mathrm{d}x \\ & + \int_{\Omega} [((\nabla \nabla u) \cdot V) \cdot \nabla \bar{w} + (\nabla u) \cdot (\nabla \nabla \bar{w}) \cdot V] \,\mathrm{d}x \\ & + \int_{\Gamma} [(\nu \cdot \nabla u^-)\, (V \cdot \nabla \bar{w}^-) + (V \cdot \nabla u^-)\, (\nu \cdot \nabla \bar{w}^-)] \,\mathrm{d}\sigma. \end{aligned}$$

Adding the contributions, using that u and $\bar{w}$ satisfy the (source-free) Helmholtz equation in Ω, leads to the simplification

$$\begin{aligned} (3.18) \qquad & \int_{\Omega} (\nabla u \cdot \nabla \bar{w} - q_1\, u \bar{w})\, \nabla \cdot V \,\mathrm{d}x - \int_{\Omega} ((\nabla V + (\nabla V)^T) \nabla u) \cdot \nabla \bar{w} \,\mathrm{d}x \\ & = - \int_{\Gamma} \nabla u^- \cdot \nabla \bar{w}^- \, \nu \cdot V \,\mathrm{d}\sigma + \int_{\Gamma} q_1\, u^- \bar{w}^- \, \nu \cdot V \,\mathrm{d}\sigma \\ & \quad + \int_{\Gamma} [(\nu \cdot \nabla u^-)\, (V \cdot \nabla \bar{w}^-) + (V \cdot \nabla u^-)\, (\nu \cdot \nabla \bar{w}^-)] \,\mathrm{d}\sigma. \end{aligned}$$

We repeat these calculations for the integral over $\Theta \setminus \overline{\Omega}$. Because V vanishes on $\partial\Theta$, the boundary integrals over $\partial\Theta$ are zero; because V vanishes in open neighborhoods of the support of f and Σ, the volume integral over the support of f vanishes as well as the integral over Σ. Thus,

$$\begin{aligned} (3.19) \qquad & \int_{\Theta \setminus \overline{\Omega}} (\nabla u \cdot \nabla \bar{w} - q_2\, u \bar{w})\, \nabla \cdot V \,\mathrm{d}x - \int_{\Theta \setminus \overline{\Omega}} ((\nabla V + (\nabla V)^T) \nabla u) \cdot \nabla \bar{w} \,\mathrm{d}x \\ & = \int_{\Gamma} \nabla u^+ \cdot \nabla \bar{w}^+ \, \nu \cdot V \,\mathrm{d}\sigma - \int_{\Gamma} q_2\, u^+ \bar{w}^+ \, \nu \cdot V \,\mathrm{d}\sigma \\ & \quad - \int_{\Gamma} [(\nu \cdot \nabla u^+)\, (V \cdot \nabla \bar{w}^+) + (V \cdot \nabla u^+)\, (\nu \cdot \nabla \bar{w}^+)] \,\mathrm{d}\sigma. \end{aligned}$$

Substituting (3.18) and (3.19) into (3.17) results in

$$\begin{aligned} D\mathcal{J}(\Omega, q_1, q_2)\, V = \mathrm{Re}\, \Big\{ & \int_\Gamma \nabla u^+ \cdot \nabla \bar{w}^+ \, \nu \cdot V \, \mathrm{d}\sigma - \int_\Gamma q_2 \, u^+ \bar{w}^+ \, \nu \cdot V \, \mathrm{d}\sigma \\ & - \int_\Gamma \nabla u^- \cdot \nabla \bar{w}^- \, \nu \cdot V \, \mathrm{d}\sigma + \int_\Gamma q_1 \, u^- \bar{w}^- \, \nu \cdot V \, \mathrm{d}\sigma \\ & - \int_\Gamma [(\nu \cdot \nabla u^+)\, (V \cdot \nabla \bar{w}^+) + (V \cdot \nabla u^+)\, (\nu \cdot \nabla \bar{w}^+)] \, \mathrm{d}\sigma \\ & + \int_\Gamma [(\nu \cdot \nabla u^-)\, (V \cdot \nabla \bar{w}^-) + (V \cdot \nabla u^-)\, (\nu \cdot \nabla \bar{w}^-)] \, \mathrm{d}\sigma \, \Big\}, \end{aligned}$$

and using our boundary conditions, we obtain

$$D\mathcal{J}(\Omega, q_1, q_2)\, V = \mathrm{Re}\, \Big\{ \int_\Gamma (q_1 - q_2)\, u \bar{w}\, \nu \cdot V \, \mathrm{d}\sigma \Big\} = \int_\Gamma \rho v \, \mathrm{d}\sigma, \tag{3.20}$$

where $V = v\nu$.

With the explicit expression of ρ, we can derive the corresponding gradient flow in the level set formulation as in (2.10).

$$\begin{aligned} \frac{\partial \phi}{\partial t} &= -v(x,t)\, |\nabla \phi|, \\ &= \mathrm{Re}\{(q_1(x) - q_2(x))\, u(x,t) \bar{w}(x,t)\}\, |\nabla \phi|. \end{aligned} \tag{3.21}$$

For convenience, the narrowband method is implemented with DRLSE formulation (2.13)

$$\mathcal{R}_p(\phi) = \int_\Theta \frac{1}{2} (|\nabla \phi - 1)^2 \, \mathrm{d}x.$$

The final evolution is then given by

$$\frac{\partial \phi}{\partial t} = \left(\nabla^2 \phi - \nabla \cdot \frac{\nabla \phi}{|\nabla \phi|} \right) + \mathrm{Re}\{(q_1(x) - q_2(x))\, u(x,t) \bar{w}(x,t)\}\, |\nabla \phi|. \tag{3.22}$$

4. The shape derivative in segmentation. In this section, we begin with the wavespeed optimization, modelling the data with solutions of the Helmholtz equation, to obtain an "initial" wavespeed model. After that, we introduce the imaging-based shape functional and the corresponding shape derivative to perform domain segmentation.

4.1. Gradient flow of wavespeed optimization. We consider the one-parameter family of models q_t with $q_0 = q$, and a set of source functions $(f_k(x))_{k=1}^N$. We let D and Θ be as before. Suppose that $(u_{k,t}(x))_{k=1}^N$ satisfy the variational equations

$$b(q_t; u_{k,t}, v) = s_k(v) \quad \text{for all } v \in H^1(\Theta), \tag{4.1}$$

with

$$b(q_t; u_{k,t}, v) = \int_\Theta \left(\nabla u_{k,t} \cdot \nabla \bar{v} - q_t \, u_{k,t} \bar{v} \right) \, \mathrm{d}x, \tag{4.2}$$

and

$$s_k(v) = \int_{\Theta \setminus \overline{D}} f_k \, \bar{v} \, \mathrm{d}x - \int_{\partial \Theta} (\Lambda_e u)\, \bar{v} \, \mathrm{d}\sigma. \tag{4.3}$$

We write the solution $u_{k,t}$ restricted to Σ as an operator $\mathcal{S}(q_t)$ acting on f_k, and introduce the objective functional,

$$\mathcal{J}(q_t) = \frac{1}{2}\sum_{k=1}^{N} \|\mathcal{P}\left(\mathcal{S}(q_t)f_k - d_{f,k}\right)\|^2_{L^2(\Sigma)}; \tag{4.4}$$

here, $(d_{f,k}(x))_{k=1}^N$ represent the data. Following the same process as in Section 3, we introduce the augmented functionals with $v = (v_k(x))_{k=1}^N$ and Lagrange multipliers $(w_k(x))_{k=1}^N$,

$$\mathcal{L}(q_t; v, w) = \mathcal{J}(q_t) + \sum_{k=1}^{N} \mathrm{Re}\ \left(b(q_t; v_k, w_k) - s_k(w_k)\right). \tag{4.5}$$

Then

$$\frac{\mathrm{d}}{\mathrm{d}t}\mathcal{L}(q_t, u_k, w)\ \Big|_{t=0} = \sum_{k=1}^{N} \mathrm{Re}\ \ \frac{\mathrm{d}}{\mathrm{d}t} b(q_t; u_k, w_k)\ \Big|_{t=0}, \tag{4.6}$$

if $(\bar{w}_k)_{k=1}^N$ solve adjoint state equations of the type (3.16), with f replaced by f_k. We then evaluate

$$\frac{\mathrm{d}}{\mathrm{d}t} b(q_t; u_k, w_k)\ \Big|_{t=0} = -\int_{\Theta} u_k \bar{w}_k\ \frac{\mathrm{d}}{\mathrm{d}t} q_t\ \Big|_{t=0}\ \mathrm{d}x \tag{4.7}$$

and identify

$$\frac{\mathrm{d}}{\mathrm{d}t} q_t\ \Big|_{t=0} \quad \text{with} \quad v.$$

Thus

$$-\sum_{k=1}^{N} \mathrm{Re}\ \int_{\Theta} u_k \bar{w}_k\, v\, \mathrm{d}x =: (\rho, v)_{L^2(\Theta)}, \tag{4.8}$$

that is, $\rho = -\sum_{k=1}^{N} \mathrm{Re}\ u_k \bar{w}_k$. This gives the usual gradient flow for seismic full waveform inversion.

We can introduce a basis $\{\psi_\alpha\}_{\alpha=1}^{N_q}$ adapted to Ω to represent the wavespeed model; that is, we write

$$q(x) = \sum_{\alpha=1}^{N_q} \gamma_\alpha \psi_\alpha(x).$$

Following this representation, we replace the right-hand side of (4.7) by

$$-\sum_{\alpha=1}^{N_q} \left(\int_{\Theta} u_k \bar{w}_k\, \psi_\alpha\, \mathrm{d}x\right) \frac{\mathrm{d}}{\mathrm{d}t}\gamma_{\alpha,t}\ \Big|_{t=0},$$

and identify

$$\frac{\mathrm{d}}{\mathrm{d}t}\gamma_{\alpha,t}\ \Big|_{t=0} \quad \text{with} \quad v \in \mathbb{R}^{N_q}.$$

The gradient method is implemented by iteratively updating the wavespeed parameter q as

$$q_{n+1} = q_n + \tau_n \rho_n. \tag{4.9}$$

During this procedure, we imbed a total variation (TV) regularization into the updating scheme. The result is a projected gradient iteration algorithm:

$$\begin{cases} \widetilde{q}_{n+1} = q_n + \tau_n \rho_n, \\ q_{n+1} = P_{TV}(\widetilde{q}_{n+1}) \\ \qquad = \operatorname{argmin}_q \|q\|_{BV} + \dfrac{\lambda}{2}\|q - \widetilde{q}_{n+1}\|_2^2, \end{cases} \tag{4.10}$$

where λ is a penalty function weight. We summarize this regularization method in the Appendix.

4.2. Shape functional for segmentation. We treat the available wavespeed model as an image, that is, $I(x) := q(x)$. In this subsection, $I(x) : \ \Theta \to \mathbb{R}$ is a given image intensity function. We introduce segmentation via an edge-based active contour model with a distance regularized level set implementation [21].

The energy functional contains an edge detector function, which takes on small values near boundaries,

$$g = \frac{1}{1 + \beta |\nabla I|^2}. \tag{4.11}$$

We may use a convolution of the image with a Gaussian kernel to mitigate any noise.

We define the energy functional by

$$\mathcal{J}(\Omega) = \gamma \int_\Gamma g \, \mathrm{d}\sigma + \mu \int_\Omega g \, \mathrm{d}x, \tag{4.12}$$

where $\gamma, \mu > 0$ represent the weight parameters. According to [41], the shape derivative can be written by

$$D\mathcal{J}(\Omega)\, V = \int_\Gamma g(\gamma\kappa + \mu) v \, \mathrm{d}\sigma = \int_\Gamma \rho v \, \mathrm{d}\sigma,$$

where $V = v\nu$, κ is the mean curvature.

Given a level set function, $\phi : \ \Theta \to \mathcal{R}$ and DRLSE regularization term $\mathcal{R}_p(\phi)$ as in (2.13), the functional takes the form

$$\mathcal{J}(\Omega) = \int_\Theta p(|\nabla\phi|) \, \mathrm{d}x + \gamma \int_\Theta g\delta(\phi)|\nabla\phi| \, \mathrm{d}x + \mu \int_\Theta gH(\phi) \, \mathrm{d}x. \tag{4.13}$$

where δ and H denote the Dirac measure and the Heaviside function.

The energy functional can be interpreted as: given an observed image $I(x)$, an optimal boundary Γ is to be found. The first term acts to avoid the re-initialization step. The second term signifies the energy along the zero level, which is minimized when the zero level set encounters the boundary. The third term represents a weighted area of the region Ω. So the model works as an edge detector to locate the final boundary at the points of maxima $\nabla I(x)$.

The level set evolution to the optimal boundary is then described by

$$\begin{aligned} \frac{\partial\phi}{\partial t} &= \nabla \cdot \left(p'(|\nabla\phi|) \frac{\nabla\phi}{|\nabla\phi|} \right) + g\delta(\phi) \left(\gamma \nabla \cdot \frac{\nabla\phi}{|\nabla\phi|} - \mu \right) \\ &= \left(\nabla^2\phi - \nabla \cdot \frac{\nabla\phi}{|\nabla\phi|} \right) + g\delta(\phi) \left(\gamma \nabla \cdot \frac{\nabla\phi}{|\nabla\phi|} - \mu \right). \end{aligned} \tag{4.14}$$

For the implementation we resort to an implicit-explicit finite difference scheme. As in (2.16), we apply an implicit scheme to the mean curvature term and an explicit scheme to the other terms in the level set time discretization form.

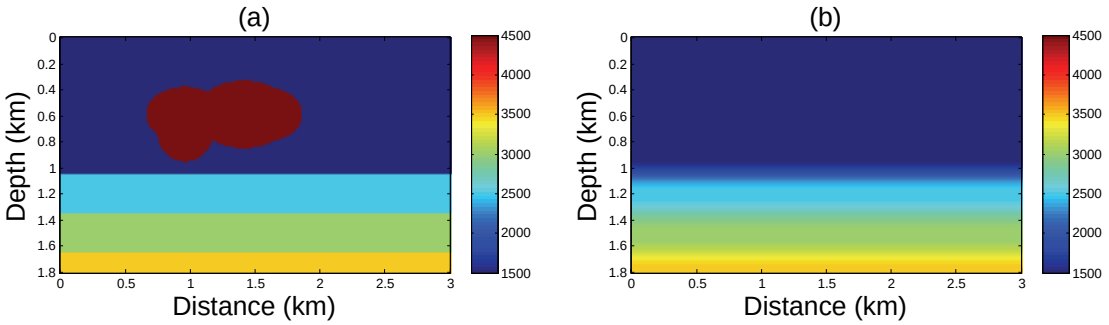

FIG. 2. *(a): The true wavespeed model. (b): Initial wavespeed for optimization.*

5. Algorithm and numerical experiments. We carry out numerical experiments with a 2-dimensional model. The model is depicted in Figure 2 (a) and consists of a body with a high wavespeed and boundary Γ and surrounding layers. The wavespeed varies from 1500 m/s to 4500 m/s. We consider 41 point sources (f_k) evenly spaced at the (top) surface and 5 frequencies, $1.0, 2.0, 4.0, 5.7, 8.0$ Hz. The field is observed at 81 evenly spaced receivers at the (top) surface. The initial model for our iteration procedure is illustrated in Figure 2 (b). The computational mesh used for solving the Helmholtz equation is a 121 by 201 grid with spatial stepsize 15m.

Wavespeed optimization, initiation. As a first test, we carry out the q iteration to optimize the wavespeed. We take as an initial model, a smoothed version of the true model, which does not contain the information about the body. Five frequencies are employed sequentially from low to high. For convenience, the algorithm runs for 10 iterations each frequency when the functional no longer reduces in value much. Figure 3 displays the final reconstruction results and two wavespeed profile' comparisons at distances of 0.45 km, 1.5 km. Figure 4 shows the reconstructed results using TV regularization. These two numerical results show that the first step of wavespeed optimization alone doesn't perform very well comparable to the true model. As expected, the sharp edges of the wavespeed model are better resolved with the TV regularization.

Segmentation. In the next step, as discussed in Section 4, we employ the edge-based segmentation to estimate the shape of the body. We start with a rectangle which includes the body as in Figure 5 (a), and perform the shape evolution until the functional no longer reduces in value much.

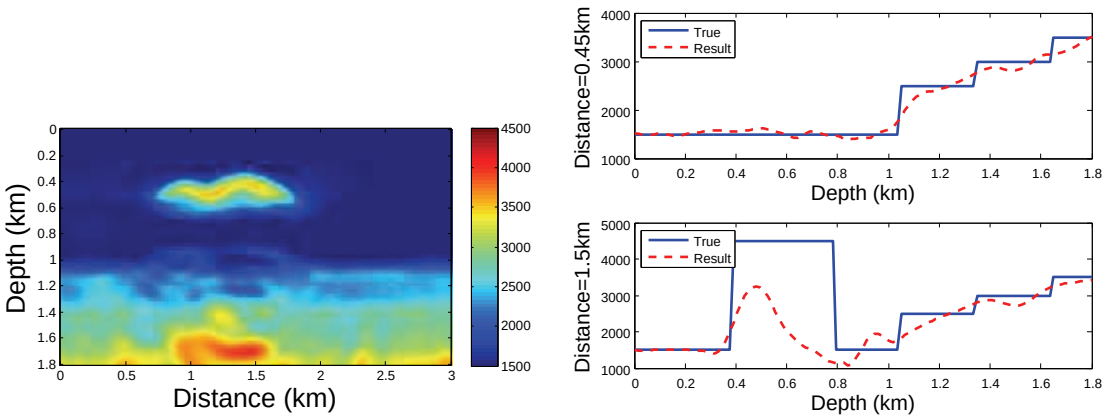

FIG. 3. *The wavespeed optimization result (left) and wavespeed profiles (right) at distances of 0.45 km, 1.5 km.*

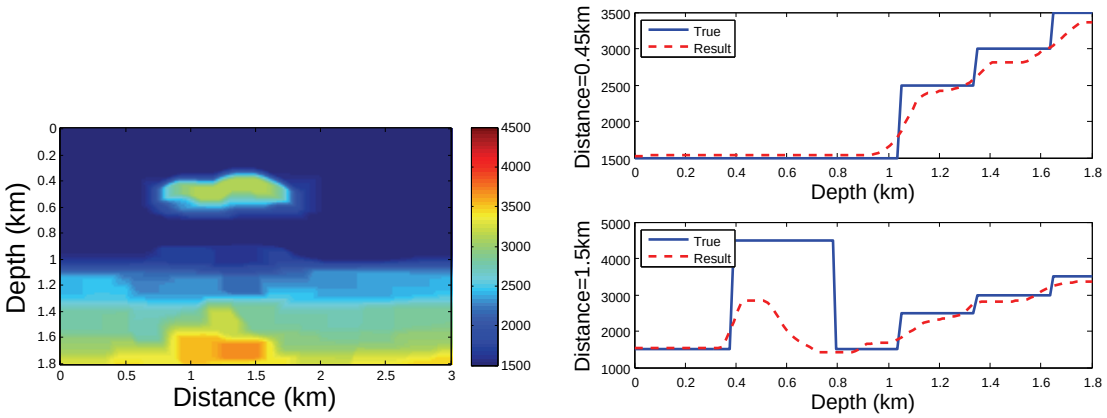

FIG. 4. *The wavespeed optimization with TV regularization result (left) and wavespeed profiles (right) at distances of 0.45 km, 1.5 km.*

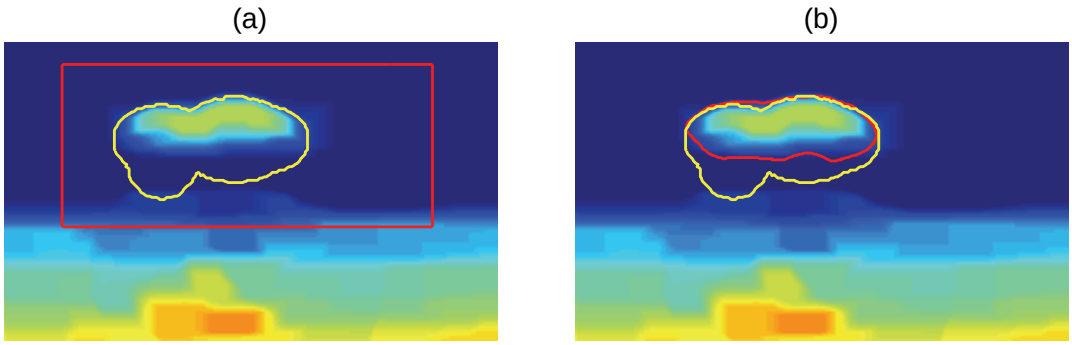

FIG. 5. *Level set boundary evolution (red) compared with the true data boundary (yellow). The initial zero level set, and final the zero level are shown at (a), (b).*

The result is shown in Figure 5 (b). The final shape is used as the initial shape Ω_0 in the shape optimization procedure.

Shape optimization, alternating wavespeed optimization. We employ the iterative level set evolution method with descent direction deduced from the shape derivative in Section 3. The boundary and average wavespeed of the body are updated each step. We use the same five frequencies sequentially from low to high, with 10 iterations for each frequency. The results are displayed in Figures 6 and 7. Note that we use a fixed background equal to the initial model and the body wavespeed is always assumed to be constant. Since data is only measured at the (top) surface, we have to expect a better reconstruction of the top boundary than the bottom boundary. Our numerical tests demonstrate the problem. We can get almost an exact match with the top boundary. The bottom part of the boundary is close to the one of the true model but it is not fully resolved.

Wavespeed optimization, closing the loop. We carry out, again, the q iteration on the computational domain using the result obtained in the shape optimization as the initial model. The optimization is performed by smoothing the initial model and the final result is shown in Figure 8 (a). The optimization is also carried out by employing the TV regularization method, which is shown in Figure 8 (b). Two wavespeed profiles at distances of 0.45 km and 1.5 km are plotted for comparison with the true model in Figure 9.

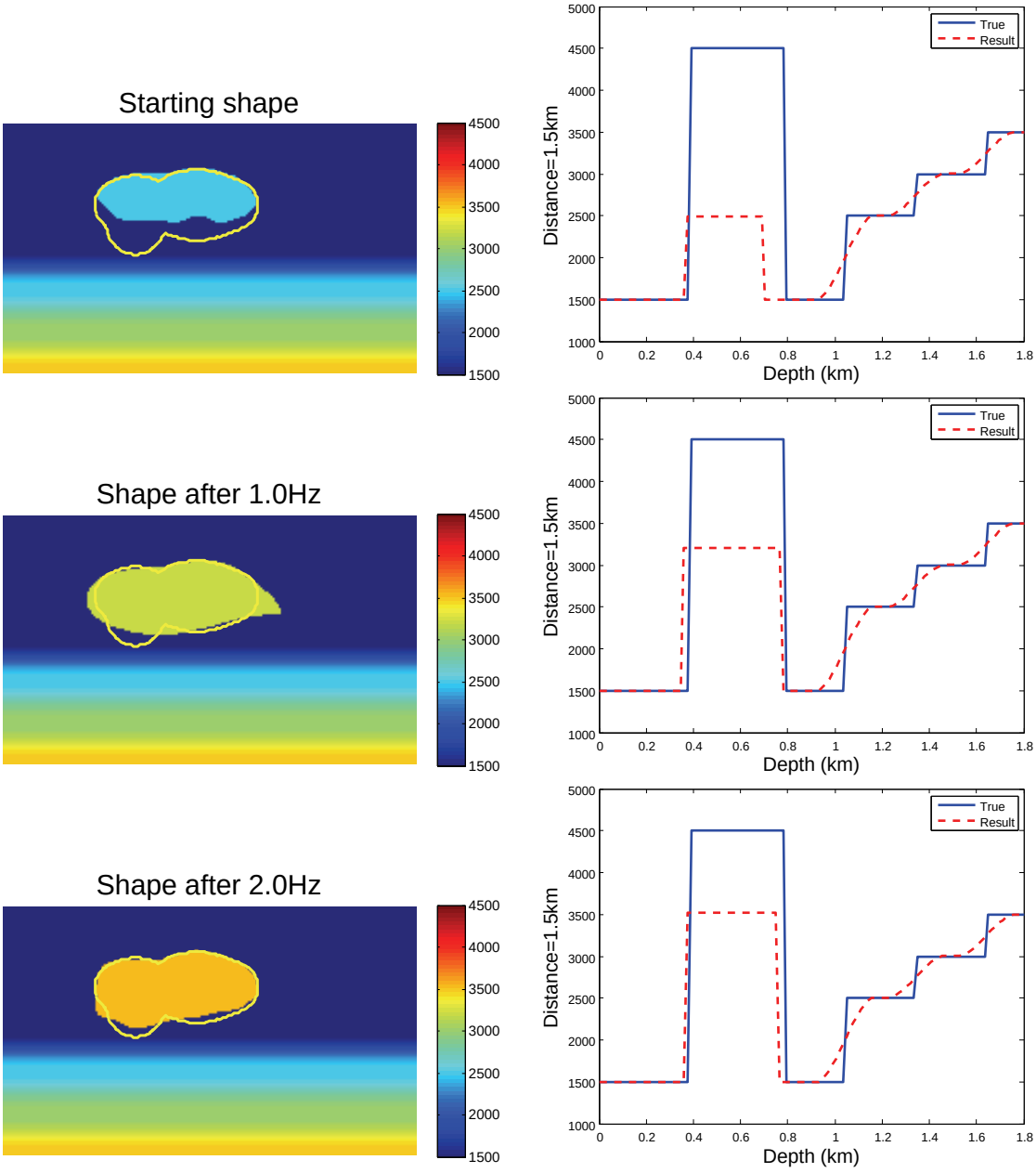

FIG. 6. *The shape optimization boundary evolution after each frequency (left) and wavespeed profiles (right) at distances of 1.5 km.*

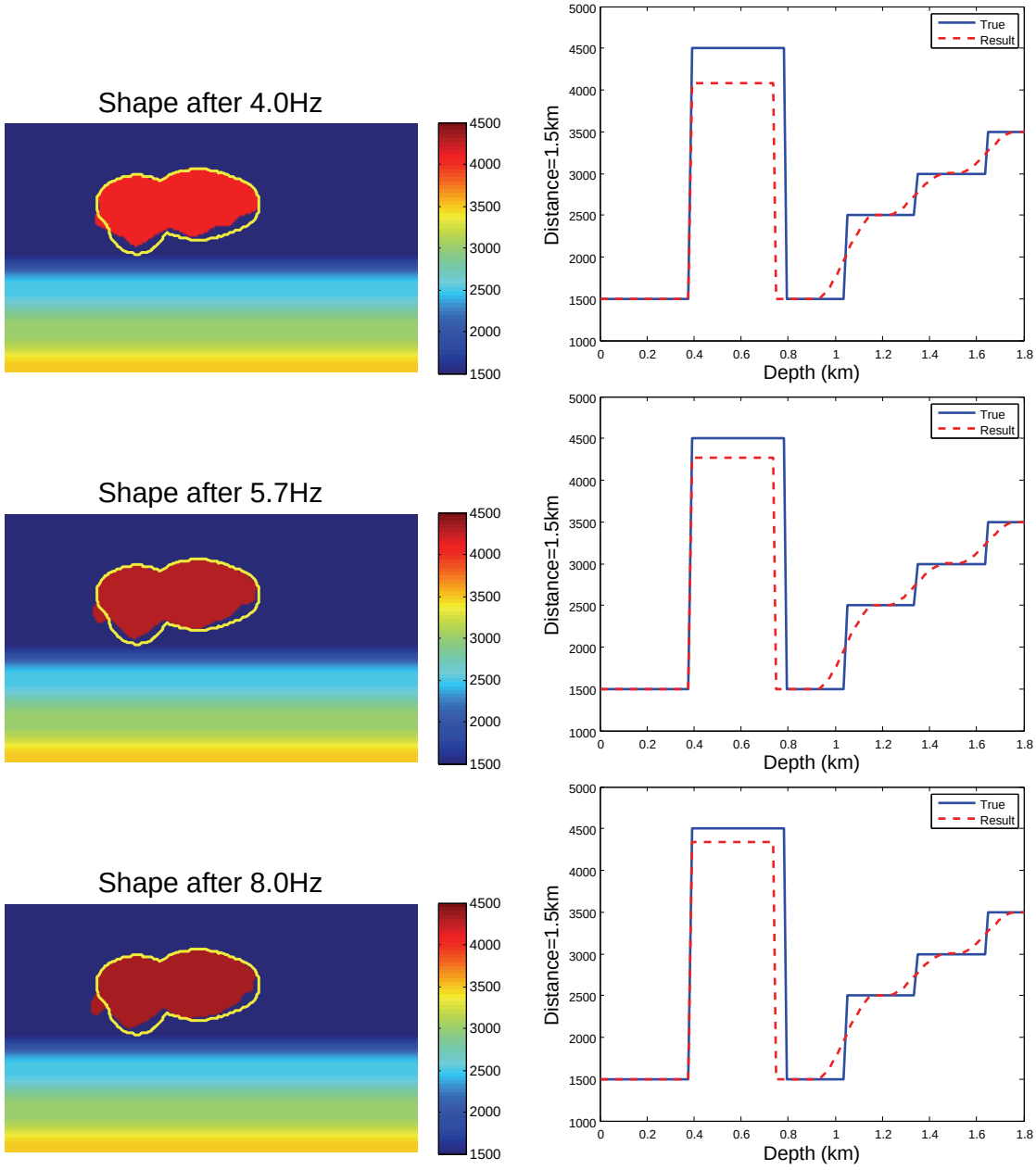

FIG. 7. *The shape optimization boundary evolution after each frequency (left) and wavespeed profiles (right) at distances of 1.5 km.*

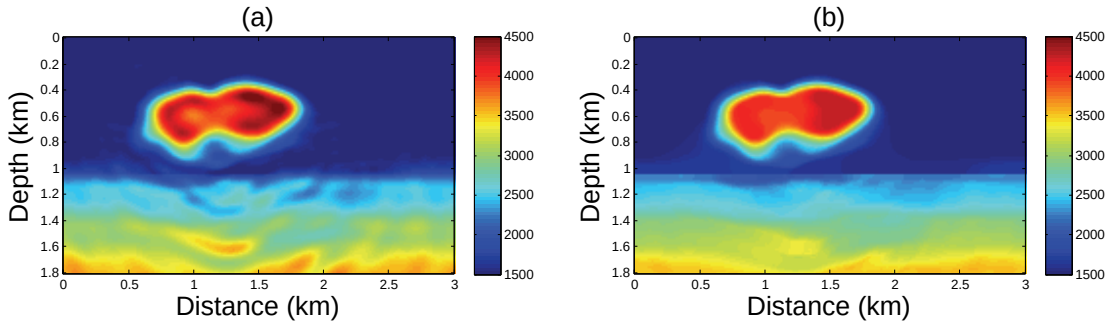

FIG. 8. *The final wavespeed optimization result (a): without TV regularization. (b) with TV regularization.*

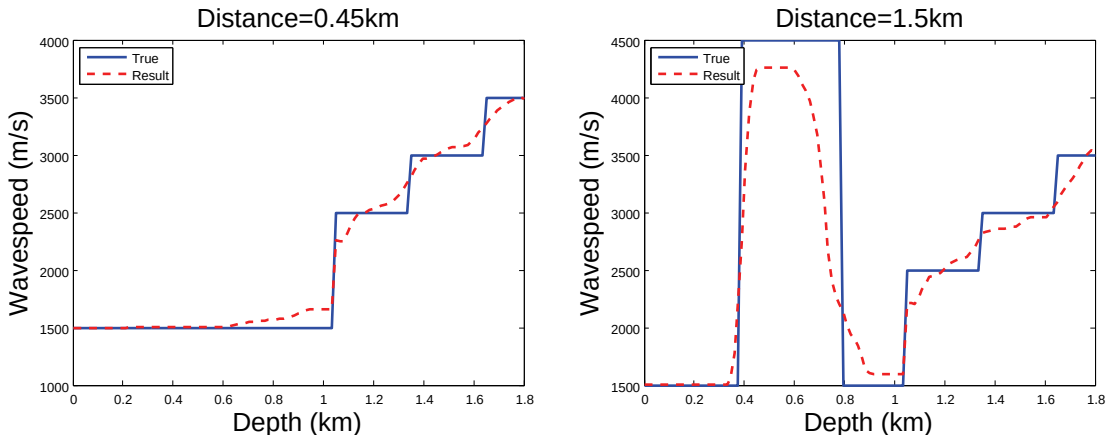

FIG. 9. *The final wavespeed profiles at distances of 0.45 km (left) and 1.5 km (right).*

6. Conclusion. In this paper, we propose a shape optimization framework for full waveform inversion in reflection seismology based on an adaptive decomposition into subdomains. The algorithm consists of three components including domain segmentation and shape deformation, alternating with constrained wavespeed optimization. We consider the gradient flow and level set method based on shape derivatives of the associated objective functionals. The performance of our approach and algorithm is demonstrated by numerical experiments.

Appendix. Total Variation regularization.

Total variation (TV) regularization is built in the wavespeed updating scheme to enforce the production of blocky or piecewise constant wavespeed data. Here, we summarize the procedure. The readers are referred to [26, 35] for more details.

The BV norm is defined as

$$\|q\|_{BV} = \int_\Theta |\nabla q| \, \mathrm{d}x = \sup \left\{ \int_\Theta q \ \operatorname{div} g \mathrm{d}x \mid g \in C_0^1(\Theta, \mathbb{R}), \|g\|_\infty \leq 1 \right\}. \tag{A.1}$$

The space $BV(\Theta)$ is the space of functions of bounded variation. The TV regularization takes the form of a minimization problem with functional

$$\|q\|_{BV} + \frac{\lambda}{2}\|q - f\|_2^2, \tag{A.2}$$

where f is known. Here, as in (4.10), f is obtained from an iteration procedure. This functional appears in the classical total variation based image restoration problem, known as Rudin-Osher-Fatemi (ROF) model.

To solve the ROF model, we use the newly developed split Bregman algorithm which was proposed in [13]. In this algorithm, one introduces an auxiliary variable, $d = \nabla q$, and transforms $\|q\|_{BV}$ into an l_1 norm of d. This leads to a constrained l_1 minimization,

$$\min_q \left\{ \|d\|_1 + \frac{\lambda}{2}\|q - f\|_2^2 \right\} \quad \text{such that } d = \nabla q,$$

which can be straightforwardly implemented with an efficient soft thresholding operation. The related unconstrained minimization problem is obtained by adding a penalty term to the functional according to

$$\|d\|_1 + \frac{\lambda}{2}\|q - f\|_2^2 + \frac{\delta}{2}\|d - \nabla q\|_2^2. \tag{A.3}$$

To obtain an efficient scheme, we introduce the Bregman iteration method [4, 26] with a Bregman parameter b_l, and iteratively solve a sequence of unconstrained problems given by

$$\begin{cases} (q_{l+1}, d_{l+1}) = \text{argmin}_{q,d}\{\ ||d||_1 + \frac{\lambda}{2}||q - f||_2^2 + \frac{\delta}{2}||d - \nabla q - b_l||_2^2\ \}, \\ b_{l+1} = b_l + (\nabla q_{l+1} - d_{l+1}), \end{cases} \tag{A.4}$$

for $l = 1, 2, ...n$. It is an alternating minimization scheme, where b_l is updated every step by adding the residual from the quadratic penalty term $\|d - \nabla q\|_2^2$. In other words, we add the residual back to enhance the image denosing. Convergence analysis of the iterative scheme is also provided in [26].

To solve the first subproblem in (A.4), we"split" the l_1 and l_2 components and perform optimization in an alternating minimization fashion:

$$\begin{cases} q_{l+1} = \text{argmin}_q\{\ \frac{\lambda}{2}||q - f||_2^2 + \frac{\delta}{2}||d_l - \nabla q - b_l||_2^2\ \}, \\ d_{l+1} = \text{argmin}_d\{\ ||d||_1 + \frac{\delta}{2}||d - \nabla q_{l+1} - b_l||_2^2\ \}, \\ b_{l+1} = b_l + (\nabla q_{l+1} - d_{l+1}). \end{cases} \tag{A.5}$$

We transform the original TV regularized problem into a sequence of unconstrained optimization problems and Bregman iteration. Amongst them, the optimal value of q can be obtained by solving the first subproblem, which involves solving the following system

$$(\lambda I - \delta\Delta)q_{l+1} = \lambda f + \delta\nabla \cdot (d_l - b_l).$$

The second subproblem is the l_1 norm minimization which can be computed componentwise using shrinkage operator

$$d_{l+1} = \text{shrink}(\nabla q_{l+1} + b_l, 1/\delta),$$

where the operator is given as

$$\text{shrink}(x, \varepsilon) = \begin{cases} x - \varepsilon & : \quad x > \varepsilon \\ 0 & : \quad -\varepsilon \le x \le \epsilon \\ x + \varepsilon & : \quad x < -\varepsilon \end{cases}.$$

Together with all the steps in (A.5), we obtain this simple but efficient algorithm.

REFERENCES

[1] D. Adalsteinsson and J.A. Sethian, *A fast level set method for propagating interfaces*, J. Comput. Phys., 118 (1995), pp. 269–277.

[2] D. Adalsteinsson and J. Sethian, *The fast construction of extension velocities in level set methods*, J. Comput. Phys., 148 (1999), pp. 2–22.

[3] F. Almgren and J.E. Taylor, *Optimal geometry in equilibrium and growth*, Fractals, 3 (1995), pp. 713–723.
[4] L. Bregman, *The relaxation method of finding the common points of convex sets and its application to the solution of problems in convex programming*, U.S.S.R. Comput. Math. Math. Phys., 7 (1967), pp. 200–217.
[5] M. Burger, *A framework for the construction of level set methods for shape optimization and reconstruction*, Interfaces and free boundaries, 5 (2002), pp. 301–329.
[6] A. Carpio and M.-L. Rapún, *Solving inhomogeneous inverse problems by topological derivative methods*, Inverse Problems, 24 (2008), p. 045014.
[7] S. Chen, B. Merriman, S. Osher, and P. Smereka, *A simple level set method for solving stefan problems*, J. Comput. Phys., 135 (1997), pp. 8–29.
[8] A. Cohen, W. Dahmen, and R. Devore, *Adaptive wavelet techniques in numerical simulation*, in Encyclopedia of Computational Mechanics, John Wiley & Sons, 2004.
[9] R. DeVore and A. Kunoth, *Multiscale, Nonlinear and Adaptive Approximation*, Spring, 2009.
[10] O. Dorn, E.L. Miller, and C.M. Rappaport, *A shape reconstruction method for electromagnetic tomography using adjoint fields and level sets*, Inverse Problems, 16 (2000), pp. 1119–1156.
[11] G. Doğgan, P. Morin, R.H. Nochetto, and M. Verani, *Discrete gradient flows for shape optimization and applications*, Comput. Method Appl. M, 196 (2007), pp. 3898–3914.
[12] H. Federer, *Geometric Measure Theory*, Spring, 1969.
[13] T. Goldstein and S. Osher, *The split Bregman algorithm for L1 regularized problems*, Tech. Report CAM TR08-29, University of California, Los Angeles, 2008.
[14] M. Hanke, A. Neubauer, and O. Scherzer, *A convergence analysis of landweber iteration of nonlinear ill-posed problems*, Numer. Math., 72 (1995), pp. 21–37.
[15] F. Hettlich, *Fréchet derivatives in inverse obstacle scattering*, Inverse Problems, 11 (1995), pp. 371–382.
[16] B. Kaltenbacher and B. Hofmann, *Convergence rates for the iteratively regularized gauss-newton method in banach spaces*, Inverse Problems, 26 (2010), p. 035007.
[17] B. Kaltenbacher, F. Schöpfer, and T. Schuster, *Iterative methods for nonlinear ill-posed problems in banach spaces: convergence and applications to parameter identification problems*, Inverse Problems, 25 (2009), p. 065003.
[18] A. Kirsch, *The domain derivative and two applications in inverse scattering theory*, Inverse Problems, 9 (1993), pp. 81–93.
[19] R. Kress and A. Zinn, *On the numerical solution of the three dimensional inverse obstacle scattering problem*, J. Comput. Appl. Math., 42 (1992), pp. 49–61.
[20] L. Landweber, *An iteration formula for fredholm integral equations of the first kind*, Amer. J. Math., 73 (1951), pp. 615–624.
[21] C. Li, C. Xu, C. Gui, and M.D. Fox, *Distance regularized level set evolution and its application to image segmentation*, IEEE Trans. Image Process., 19 (2010), pp. 3243–3254.
[22] A. Liseno and R. Pierri, *Imaging of voids by means of a physical optics based shape reconstruction algorithm*, J. Opt. Soc. Am. A, 21 (2004), pp. 968–974.
[23] A. Litman, D. Lesselier, and F. Santosa, *Reconstruction of a two-dimensional binary obstacle by controlled evolution of a level-set*, Inverse Problems, 14 (1998), pp. 685–706.
[24] R. Malladi, Sethian J.A., and B.C. Vemuri, *Shape modeling with front propagation: A level set approach*, IEEE Transactions on Pattern Analysis and Machine Intelligence, 17 (1995), pp. 158–175.
[25] J. M. Morel and S. Solimini, *Variational methods in image segmentation*, Birkhauser Boston Inc., 1995.
[26] S. Osher, M. Burger, D. Goldfarb, J. Xu, and W. Yin, *An iterative regularization method for total variation based image restoration*, Multiscale Model. Simul., 4 (2005), pp. 460–489.
[27] S. Osher and R.P. Fedkiw, *Level set methods and dynamic implicit surfaces*, Applied Mathematical Sciences, Springer, 2003.
[28] S. Osher and J. Sethian, *Fronts propagating with curvature-dependent speed: Algorithms based on hamilton-jacobi formulations*, J. Comput. Phys., 70 (1988), p. 12?49.
[29] ———, *Level set methods for optimization problems involving geometry and constraints i. frequencies of a two-density inhomogeneous drum*, J. Comput. Phys., 171 (2001), pp. 272–288.
[30] R. Potthast, *Fréchet differentiability of boundary integral operators in inverse acoustic scattering*, Inverse Problems, 10 (1994), pp. 431–447.
[31] ———, *Fréchet differentiability of the solution to the acoustic neumann scattering problem with respect to the domain*, J. Inverse Ill-Posed Problems, 4 (1996), pp. 67–84.
[32] R.G. Pratt, *Seismic waveform inversion in the frequency domain, part 1: Theory and verification in a physical scale model*, Geophysics, 64 (1999), pp. 888–901.
[33] R.G. Pratt, C. Shin, and G.J. Hicks, *Gauss-newton and full newton methods in frequency-space seismic waveform inversion*, Geophysical Journal International, 133 (1998), pp. 341–362.
[34] C. Ramananjaona, M. Lambert, D. Lesselier, and J.P. Zolesio, *Digital-image based elasto-tomography: nonlinear mechanical property reconstruction of homogeneous gelatine phantoms*, Int J. Inf. Syst. Sci., 2 (2001), pp. 512–521.
[35] L. Rudin, S. Osher, and E. Fatemi, *Nonlinear total variation based noise removal algorithms*, Phys. D, 60 (1992), pp. 259–268.
[36] F. Santosa, *A level-set approach for inverse problems involving obstacles*, Control, Optimizat. Calculus Variat., 1 (1996), pp. 17–33.

[37] F. Schöpfer, A.K. Louis, and T. Schuster, *Nonlinear iterative methods for linear ill-posed problems in banach spaces*, Inverse Problems, 22 (2006), pp. 311–329.
[38] J.A. Sethian, *Level set methods and fast marching methods: evolving interfaces in computational geometry, fluid mechanics, computer vision, and materials science*, Cambridge Monographs on Applied and Computational Mathematics, Cambridge University Press, 1999.
[39] C. S. Shin, *Nonlinear elastic wave inversion by blocky representations*, PhD thesis, University of Oklahoma, (1988).
[40] L. Sirgue and R.G. Pratt, *Efficient waveform inversion and imaging: A strategy for selecting temporal frequencies*, Geophysics, 69 (2004), pp. 231–248.
[41] J. Sokolowski and J.-P. Zolesio, *Introduction to shape optimization: shape sensitivity analysis*, vol. 16 of computational mathematics, Springer-Verlag, Berlin, 1992.
[42] M. Sussman, P. Smereka, and S. Osher, *A level set approach for computing solutions to incompressible two-phase flow*, J. Comput. Phys., 114 (1994), pp. 146–159.
[43] W.W. Symes, *The seismic reflection inverse problem*, Inverse Problems, 25 (2009), p. 123008.
[44] G. Uhlmann, *Electrical impedance tomography and calderón's problem*, Inverse Problems, 25 (2009), p. 123011.
[45] J. Virieux and S. Operto, *An overview of full-waveform inversion in exploration geophysics*, Geophysics, 74 (2009), pp. WCC1–WCC26.